Multicomponent Hydrogen/ Hydrocarbon Separation by MFI-Type Zeolite Membranes

Junhang Dong and Y. S. Lin
Dept. of Chemical Engineering, University of Cincinnati, Cincinnati, OH 45221

Wei Liu
Science & Technology Division, Corning Inc., Corning, NY 14831

Separation of an eight-component simulated refinery gas mixture including hydrogen (~ 84 mol %) and light hydrocarbons (C_1-C_4, $7.5 \sim 0.3$ mol %) by α-alumina-supported polycrystalline MFI zeolite membranes was studied at $25-500$°C and feed pressures of 0.1−0.4 MPa. The zeolite membrane showed excellent separation properties for rejection of hydrogen from the hydrogen/hydrocarbon mixture at <100°C. At room temperature and atmospheric pressure on both feed and permeate sides, hydrogen permeation rate is almost zero, while the hydrocarbon permeation rate is $2-4\times10^{-4}$ mol·m^{-2}·s^{-1}. The zeolite membrane outperforms the microporous carbon membrane in terms of both selectivity and permeance for hydrocarbons over hydrogen. At 500°C the zeolite membrane becomes permselective for hydrogen over hydrogen (C_1-C_4). In the whole temperature range iso-butane is nonpermeable (with a permeance below the GC analysis limit) through the zeolite membrane. Separation results of the zeolite membrane can be characterized by a solution-diffusion model considering competitive adsorption of hydrocarbons over hydrogen and configurational diffusion in the zeolite pores. The MFI-type zeolite membranes showed promise for applications in separation processes for hydrogen concentration/purification from various hydrogen/hydrocarbon mixtures (at lower temperatures) and in membrane reactors for dehydrogenation reactions (at high temperatures).

Introduction

The supported polycrystalline zeolite membrane is a novel material that offers large potential applications in energy-efficient membrane processes for gas and liquid separations. During the past decade, many efforts have been reported on finding optimal conditions for high-quality membrane synthesis, understanding gas and liquid permeation/separation mechanisms, and exploring practical applications. MFI-type zeolite membranes, free of macroporous defects with thickness varying from over 50 microns to submicron, can be prepared on various porous supports by *in situ* crystallization, seeding and secondary growth, and vapor-phase transport methods (Geus et al., 1992; Jia et al., 1993; Lovallo and Tsapatsis, 1996; Yan et al., 1997; Kikuchi et al.; 1997; Dong et al., 1998). Some experimental studies on the permeation of a single-gas and binary-gas mixture have been carried out with MFI zeolite membranes (Bai et al., 1995; Bakker et al., 1996, 1997; Funke et al., 1996; Coronas et al., 1997, 1998; van de Graaf et al., 1998; Vroon et al., 1998). Light hydrocarbons (C_1-C_4) and inorganic gases were mainly used in these permeation studies, because these gases are of great interest to the industry, and the MFI zeolite has the pore size (0.55 nm) and adsorption properties favorable for the separation of such gases.

In general, the following five-step model was used to describe the gas-molecule transport through a zeolite membrane (Barrer, 1990; Bakker et al., 1996): (1) adsorption from bulk phase to zeolite external surface; (2) diffusion from surface to inside of zeolite channels; (3) diffusion inside the zeo-

Correspondence concerning this article should be addressed to Y. S. Lin.

lite channels; (4) diffusion from the zeolite channel to the external surface; and (5) desorption from the external surface to the gas phase. The actual mechanism of gas permeation through an MFI-type zeolite membrane depends on the gas adsorption properties on the zeolite. For nonadsorbing gases, molecules may directly enter the zeolite pores from the gas phase. The separation factor of a nonadsorbing gas mixture is determined by the mobility of the molecules inside the zeolite pores and the probability of the molecules entering the zeolitic pores (Lovallo et al., 1998). Gas molecules with small size and high mobility tend to permeate through the zeolite membrane, while those with larger size and lower mobility tend not to.

For strongly adsorbing gases, permeation through an MFI membrane is controlled by adsorption and/or activated diffusion, depending on the operation conditions (temperature and pressure on both sides of the membrane). The maximum value of flux with respect to temperature can be observed for strongly adsorbing gases, because the apparent activation energy is the summary of adsorption heat (negative) and diffusion activation energy (positive) (Burggraaf et al., 1998; Bakker et al., 1996). The temperature of maximum flux increases with the adsorption strength of the substance (Bakker et al., 1997).

For permeation of binary gas mixtures, when both components are nonadsorbing, the separation factor ($\alpha_{1/2} = [y_1/y_2]_p/[y_1/y_2]_f$, where y_1 and y_2 are mol fraction of components 1 and 2, respectively, and subscripts p and f refer to the permeate side and feed side, respectively) is correlated to the permselectivity ($= F_1]/[F_2]$, where F_1 and F_2 are pure gas permeances of component 1 and 2, respectively) (Lovallo et al., 1998). When one or two strongly adsorbing components are involved, there is no correlation between the permselectivity and the separation factor. For gas mixtures containing strongly adsorbing components, the separation factor strongly depends on the operation conditions, that is, temperature and pressure (Bakker et al., 1996).

Up to date data on the permeation of gas mixtures containing more than two components are very limited. Funke et al. (1996) studied the permeation of binary and ternary vapor mixtures containing *n*-octane, *iso*-octane, and *n*-hexane. They found that the permeances of the components were a strong function of other components present in the feed. This indicates that multiple-component gas permeation through a zeolite membrane is not predictable, based on either single-gas or binary-gas permeation data. No experimental data for separation and permeation of gas mixtures containing more than three components by zeolite membranes have been published so far in the literature. However, permeation measurements for gas mixtures with compositions and separation conditions relevant to the industry process are necessary for practical use of the zeolite membranes.

In this work, permeation of a simulated refinery gas stream of eight components including hydrogen and light hydrocarbons (C_1–C_4) through an α-alumina-supported MFI-type zeolite membrane was studied in a broad temperature range and under different feed-stream pressures. These results will provide not only essential data for practical applications of zeolite membranes in separation processes but also an improved fundamental understanding of multicomponent gas transport in the polycrystalline zeolite membrane, a relatively new field in separation science.

Experimental Studies

Membrane preparation and characterization

MFI-type zeolite membrane was prepared on porous α-alumina disk with a thickness of 2 mm and a disk diameter of 20 mm. The average pore diameter and porosity of the alumina support were about 0.19 μm and 45%, respectively. The coating side of the alumina support was polished well by fine sandpaper (#800) and washed in an ultrasonic bath for 10 min. Before hydrothermal treatment, the polished alumina support was dried at 40°C for two days. Tetrapropylammonium hydroxide [(TPA)OH, 1 M, Aldrich] was used as a template, and fumed silica (99.98%, Aldrich) was the silica source. Other chemicals were sodium hydroxide (NaOH, 99.99%, Aldrich) and deionized water.

The composition of the synthesis solution was 20 g SiO_2-100 mL (1 M) (TPA)OH–1.4 g NaOH–3.2 g H_2O, which was the same as that used by Vroon (1995). Three disk supports were horizontally placed on the bottom of a Teflon-lined autoclave (265-mL capacity) with the polished side facing upward. The synthesis solution was poured carefully in the autoclave to immerse the supports. Then the autoclave was sealed and heated in an oven at 180°C for 4 h. The hydrothermal treatment was repeated one more time with the same conditions after the membranes was washed and dried at 40°C overnight. After the second synthesis, the zeolite membranes were scoured by distillated water many times and then dried at 40°C in air for 2–3 days before calcination. The detailed procedure for the synthesis of the MFI zeolite membrane was provided elsewhere (Dong et al., 1998).

After being dried, the MFI zeolite membranes were examined by X-ray diffraction (XRD)(D-500, Siemens, Cu$K\alpha$ radiation) to identify the zeolite crystal phase. Prior to removal of the template, the as-synthesized MFI zeolite membranes were checked by permeation of helium (99.99%, Wright Brothers, Inc.) after the membranes were further dried at 100°C for 5 h to examine the intergrity of the membranes. The as-synthesized membranes with helium permeance of less than 1×10^{-10} $mol\cdot s^{-1}\cdot m^{-2}\cdot Pa^{-1}$ were considered to be defect free. The morphology and thickness of the zeolite layer were checked by SEM (Hitachi S-4000). The membranes were calcined in air at 450°C for 6 h to remove the template. Single-gas permeation of H_2 (99.99%, Wright Brothers, Inc.) and SF_6 (99.9%, Aldrich) was performed to examine the integrity of the zeolite membrane after calcination. The single-gas permeation setup was described in a previous paper (Dong and Lin, 1998).

Table 1. Composition of the Simulated Refinery Gas

Component	H_2	CH_4	C_2H_6	C_2H_4	C_3H_8	C_3H_6	*n*-C_4H_{10}	*i*-C_4H_{10}
Mol fraction (%)	84.48	7.59	2.51	2.52	0.75	1.45	0.4	0.3

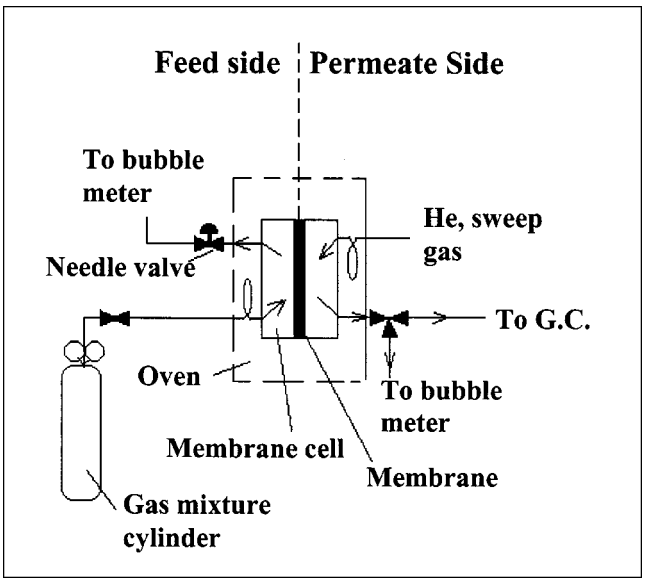

Figure 1. Multicomponent gas-permeation system.

Gas permeation and separation

The simulated refinery gas was provided by Wright Brothers, Inc., with the actual molar composition given in Table 1. Separation of the simulated refinery gas was performed by a steady-state multicomponent gas-permeation system, as shown in Figure 1. The detailed operation procedure for the permeation experiment is provided in an earlier paper (Xomeritakis and Lin, 1998). The zeolite membrane was mounted in a stainless-steel membrane cell with the membrane surface on feed side, and was sealed by silicone rubber O-rings. At 500°C graphite gaskets were used as the sealing material. The working area of the membrane was 2.8×10^{-4} m^2 when sealed by O-rings (up to 350°C) and 1.12×10^{-4} m^2 by graphite gaskets. The cell with inlet preheating coils was placed in a temperature-programmable furnace.

The feed pressure was set by the cylinder regulator, and outlet flow rate of the feed side was controlled by a needle valve. The permeate side was swept by helium under atmospheric pressure. Feed and sweep flow rates were controlled by mass flowmeters. The effluent flow rates from both the feed and permeate sides were measured by bubble flowmeters. The sweep gas flow rate and the outlet flow rate of the feed side were maintained at about 12.5 mL/min and 11.0 mL/min, respectively, unless otherwise specified. The gas-effluent composition was measured by on-line gas chromatography (GC) analysis (a HP5890, Series 11, 18 ft×0.085-in. stainless-steel column packed with 60/80 mesh silica gel, TCD detector, and helium as the carrier gas). With a sweep-gas flow rate of 12.5 mL/min, the GC analysis limit for hydrogen was about 0.5%, corresponding to a flux of 2×10^{-6} mol·m^{-2}·s^{-1}, and that for C_3 and C_4 detection was estimated at 0.03–0.01%, corresponding to a flux of about 10^{-7} mol·m^{-2}·s^{-1}. It should be noted that the flux values of the components below the GC detection limits are given as zeros in the tables of experimental data reported in this article.

Separation experiments were performed in the order of increasing temperature and feed pressure. At each test temperature or pressure, gas permeation was kept for at least one hour prior to sampling for GC analysis to assure that the system reached a steady state. In this study, flux (J_i), permeance (F_i), and separation factor (S_i) were calculated from the experimentally measured quantities by the following equations:

$$J_i = \frac{Q_p y_i}{A} \tag{1}$$

$$F_i = \frac{J_i}{P_{i,f} - P_{i,p}} \tag{2}$$

$$S_i = \frac{y_i/(1-y_i)}{x_i/(1-x_i)}, \tag{3}$$

where Q_P is total effluent flow rate of hydrogen and hydrocarbon from the permeate side; y_i and x_i are the mol fractions of hydrogen or hydrocarbon in the effluents of the feed and permeate sides, respectively; $P_{i,f}$ and $P_{i,p}$ are partial pressures of hydrogen or hydrocarbon in the feed and permeate sides calculated from the total pressure and composition in the effluent streams; and A is the active membrane permeation area.

Results and Discussion

Results

The XRD analysis confirmed that the zeolite membranes studied in this work contained zeolite films of pure MFI-type zeolite crystal structure. The membranes were defect-free before template removal as verified by the negligible helium permeance. The α-alumina-supported MFI zeolite membranes obtained in this work had a similar characteristic to those reported in our previous article (Dong et al., 1998). The thickness of the zeolite layer was 3–5 μm and the individual crystal size observed on the surface was 0.3–0.5 μm. The typical permselectivity for H_2 and SF_6 at room temperature was 150–200, indicating that no crack presented in the zeolite layer after removal of the template by calcination.

Table 2 gives the results of the separation of the simulated refinery mixture at room temperature (25°C) and under atmospheric pressure on both the feed and permeate sides. The

Table 2. Influence of Sweep Gas Flow Rate on the Separation Results*

	F_{sweep} = 5.6 mL/min		F_{sweep} = 12.1 mL/min	
Component	Flux $\times10^{-5}$ mol/s·m^2	S_i	Flux $\times10^{-5}$ mol/s·m^2	S_i
H_2	0.000	0.00	0.000	0.00
CH_4	13.67	14.4	4.650	1.66
C_2H_6	1.661	2.74	4.866	5.57
C_2H_4	4.050	7.41	9.479	12.5
C_3H_8	1.303	7.22	4.852	18.9
C_3H_6	4.491	14.8	11.53	28.7
n-C_4H_{10}	0.000	0.00	3.439	24.2
i-C_4H_{10}	0.000	0.00	0.000	0.00
Total HC flux	25.18		38.82	

*Other operating conditions: fixed feeding flow rate of 8.0 mL/min; room temperature (25°C); and atmospheric pressure (0.1 MPa) on both sides.

results were obtained at two sweep-gas flow rates, with the flow rate of the feed side outlet kept at about 8.0 mL/min. As shown, the total flux for the zeolite membrane increases from 25.18 (10^{-5} mol·m^{-2}·s^{-1}) to 38.82 (10^{-5} mol·m^{2}·s^{-1}) as the sweep-gas flow rate is raised from 5.6 mL/min to 12.1 mL/min. No hydrogen and *iso*-butane were detected at the permeate side under present conditions. It is postulated that at room temperature, the zeolitic pores are blocked by adsorbed hydrocarbons, and as a result, the nonadsorbing hydrogen is unable to permeate through the membrane. *iso*-Butane, however, was excluded by the shape-selectivity nature of the zeolite membrane. High shape-selectivity of MFI zeolite membranes for *n*-butane and *iso*-butane has been reported by several groups (Vroon et al., 1998; Coronas et al., 1998).

Increasing the sweep-gas flow rate enhances both the flux and separation factor for almost all hydrocarbons except for methane. An increase of the sweep-gas flow rate reduces the downstream partial pressure of the hydrocarbons and thus facilitates the fifth step of the permeation model, that is, desorption of the hydrogen molecules from the zeolite external surface (bottom of the zeolite layer) to the gas phase. The decrease of the methane flux and separation factor at higher sweep-gas flow rate could be due to the effect of the counter-diffusion of the sweep gas whose partial pressure in the permeate side increases with increasing sweep-gas flow rate (Bai et al., 1995). Counterdiffusion of the sweep gas (helium) has an insignificant effect on the strongly adsorbing components because helium is nonadsorbing.

Gas separation was further conducted by varying the feed-side pressure while maintaining atmospheric pressure at the permeate side. Table 3 and Figure 2 show variations of the separation factor and flux, respectively, of individual components, with the membrane upstream pressure at 75°C. The total flux increases with increasing feed-side pressure (Table 3). The fluxes of hydrogen and methane first increase with feed pressure, then decrease when pressure increases further, whereas the fluxes of hydrocarbons (C_2–C_4) increase mainly throughout the investigated pressure range (Figure 2). The separation factor of hydrogen decreases continuously from 0.096 to 0.025 as upstream pressure increases from 0.1 MPa to 0.372 MPa (Table 3). At 75°C, the zeolite pores are likely to be partially blocked by the adsorbed hydrocarbons because of the low hydrocarbon concentration. Under this condition hydrogen is able to permeate through the zeolite membrane at a very low rate.

Table 3. Effect of Feed-Side Pressure on the Separation Results (75°C)*

Component	Separation Factor, S_i			
	0.1 MPa	0.168 MPa	0.27 MPa	0.372 MPa
H_2	0.096	0.093	0.039	0.025
CH_4	1.72	2.07	2.89	1.87
C_2H_6	3.67	5.49	4.68	8.94
C_2H_4	8.26	6.12	10.1	24.8
C_3H_8	24.4	18.9	26.2	22.8
C_3H_6	24.2	16.5	59.8	66.5
n-C_4H_{10}	0	13.9	48.3	31.0
i-C_4H_{10}	0	0	0	0
H_2 flux, 10^{-5} mol/m^2·s	37.31	44.96	32.90	27.85
Total HC flux, 10^{-5} mol/m^2·s	62.34	77.10	116.2	147.1

*Other operating conditions: 0.1 MPa at the sweep side; sweep gas flow rate of 12.8 mL/min; and feeding flow rate of 11.1 mL/min.

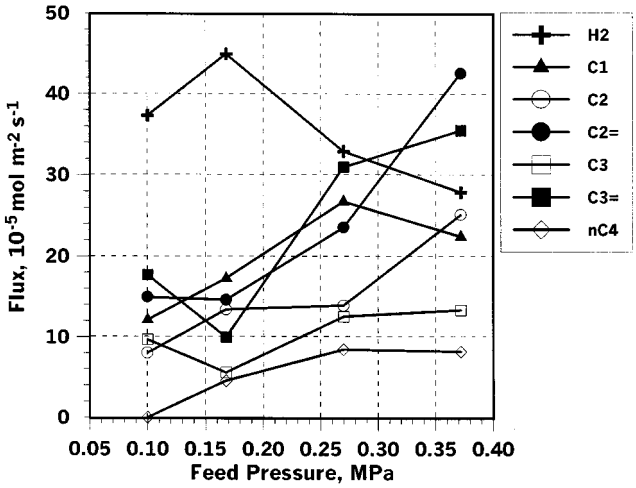

Figure 2. Effect of feed-side pressure on the gas permeation (75°C).

Increasing upstream pressure has the opposite effect on the permeation of the nonadsorbing hydrogen and that of the adsorbing hydrocarbon component. On the one hand, an increase in feed pressure provides larger partial pressure differences across the membrane for hydrogen and methane that may increase their permeation. On the other hand, increasing feed pressure raises the partial pressures of the strongly adsorbing hydrocarbons, which enhances their adsorption on the zeolite and further blocks the zeolitic pores, resulting in inhibition of the permeation of hydrogen and methane. In the first stage of feed pressure increase, the positive effect (increases in driving force) on the permeation of hydrogen and methane might overmatch the inhibiting effect (pore blocking by adsorbed hydrocarbons), and thus an increase in hydrogen and methane fluxes was observed.

Gas separation was systematically studied over a temperature range of 25–300°C at four different feed pressures, 0.1, 0.168, 0.27 and 0.372 MPa. The downstream side of the zeolite membrane was maintained at atmospheric pressure and swept by helium gas. As noted before, the sweep gas and the feed-side outlet flow rates were maintained at around 12.5 and 11 mL/min, respectively. The experimental results are summarized in Tables 4–7 and Figures 3–6. Tables 4–7 list separation factors of individual components at different temperatures under a constant feed pressure, while Figures 3–6 show fluxes of corresponding components. Similar effects of the feed pressure on gas permeation are observed at temperatures 25, 105, and 150°C, but very different results were obtained at 200 and 300°C. At temperatures over 200°C, adsorption of light hydrocarbons on MFI zeolite becomes negligible and the permeation becomes gaseous diffusion-controlled. At 200 and 300°C, fluxes for all components increased with an increase in the upstream pressure, except for *iso*-butane, which was not detectable at the permeate side in all cases.

Table 4. Results of Gas Separation at Different Temperatures and Under Feed Pressure of 0.1 MPa*

Component	Separation factor, S_i				
	25°C	75°C	105°C	200°C	300°C
H_2	0	0.096	0.172	1.88	1.00
CH_4	1.26	1.72	2.34	0.63	0.88
C_2H_6	6.45	3.67	3.05	0.47	1.50
C_2H_4	9.38	6.26	5.44	1.15	1.09
C_3H_8	40.6	24.4	18.6	0	0.81
C_3H_6	66.9	24.2	9.79	0	1.39
n-C_4H_{10}	0	0	0	0	0
i-C_4H_{10}	0	0	0	0	0
H_2 flux, 10^{-5} mol/m^2·s	0	37.31	98.85	151.9	382.7
Total HC flux, 10^{-5} mol/m^2·s	29.47	62.34	89.84	15.25	70.57

*Other operating conditions: fixed sweep-side pressure of 0.1 MPa; feed flow rate of 10.5–11.5 mL/min; and sweep gas flow rate of 12.0–13.0 mL/min.

Table 5. Results of Gas Separation Under Feed-Side Pressure of 0.168 MPa*

Component	Separation Factor, S_i					
	25°C	75°C	105°C	150°C	200°C	300°C
H_2	0	0.093	0.18	2.00	2.90	1.33
CH_4	1.80	2.07	2.07	0.62	0.45	0.75
C_2H_6	4.69	5.49	4.12	0.43	0.28	1.20
C_2H_4	15.9	6.12	7.21	1.04	0.70	0.61
C_3H_8	37.3	18.9	7.04	0	0	1.23
C_3H_6	39.5	16.5	7.63	0	0	0.78
n-C_4H_{10}	0	13.9	0	0	0	0
i-C_4H_{10}	0	0	0	0	0	0
H_2 flux, 10^{-5} mol/m^2·s	0	44.96	94.81	183.4	249.4	601.3
Total HC flux, 10^{-5} mol/m^2·s	32.49	77.13	81.06	17.47	16.93	87.56

*Other operating conditions: fixed sweep-side pressure of 0.1 MPa; feed flow rate of 10–11 mL/min; and sweep gas flow rate of 12.5–13.5 mL/min.

Table 6. Results of Gas Separation at Different Temperatures Under Feed Pressure of 0.27 MPa*

Component	Separation Factor, S_i					
	25°C	75°C	105°C	150°C	200°C	300°C
H_2	0	0.039	0.17	0.50	1.24	1.83
CH_4	1.44	2.89	1.90	1.17	0.71	0.55
C_2H_6	3.21	4.68	5.21	0.74	0.39	1.73
C_2H_4	8.79	10.1	7.31	2.95	1.05	0.18
C_3H_8	42.1	26.2	6.66	4.05	2.30	1.17
C_3H_6	56.6	59.8	10.1	3.78	1.58	0.41
n-C_4H_{10}	72.8	48.3	5.62	6.58	0	0
$i-C_4H_{10}$	0	0	0	0	0	0
H_2 flux, 10^{-5} mol/m^2·s	0	32.90	147.1	161.80	233.70	1323
Total HC flux, 10^{-5} mol/m^2·s	43.87	116.2.w0	124.2	56.57	35.15	160.7

*Other operating conditions: fixed sweep-side pressure of 0.1 MPa; feed flow rate of 13.0–15.0 mL/min; and sweep gas flow rate of 10.0–12.0 mL/min.

Table 7. Results of Gas Separation at Different Temperatures and Under Feed Pressure of 0.372 MPa*

Component	Separation Factor, S_i					
	25°C	75°C	105°C	150°C	200°C	300°C
H_2	0	0.025	0.19	1.13	1.33	2.08
CH_4	1.57	1.87	1.46	0.62	0.51	0.42
C_2H_6	5.78	8.94	3.92	0.82	0.37	3.65
C_2H_4	11.0	24.8	6.81	1.14	1.28	0.10
C_3H_8	21.1	22.8	6.97	0.98	1.94	0.89
C_3H_6	53.3	66.5	17.5	2.32	2.19	0.32
n-C_4H_{10}	69.3	31.0	7.68	1.39	0	0.53
i-C_4H_{10}	0	0	0	0	0	0
H_2 flux, 10^{-5} mol/m^2·s	0	27.85	171.0	361.9	314.6	2262
Total HC flux, 10^{-5} mol/m^2·s	49.91	147.1	131.0	59.54	44.74	272.7

*Other operating conditions: fixed sweep-side pressure of 0.1 MPa; feed flow rate of 12.5–15.5 mL/min; and sweep gas flow rate of 10–12 mL/min.

As explained previously, under each feed pressure no *iso*-butane was detected throughout the temperature range because of the shape-exclusion effect. At room temperature, hydrogen was not detectable in the whole feed pressure range studied. Permeation of hydrogen is inhibited by the adsorbed hydrocarbons in the zeolitic pores at low temperatures, and increases rapidly with increasing temperature. The hydrocarbon fluxes exhibit a maximum, followed by a minimum as temperature increases from 25 to 300°C, as clearly shown in Figures 3–6. The temperature dependency of the hydrocarbon fluxes in this study is consistent with that of the pure components reported by Bakker et al. (1996 and 1997).

Table 8 shows gas separation results at 500°C with feed pressure of 0.168 and 0.27 MPa. At 500°C the zeolite membrane becomes permselective to hydrogen. This is very different from the results observed at the low temperatures. At the high temperature, the separation factor for hydrogen is over 3 under both feed pressures. All C_3 and C_4 were not de-

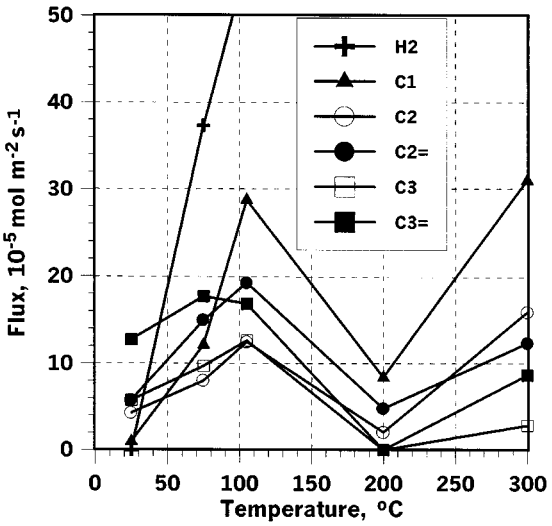

Figure 3. Gas-permeation fluxes under feed-side pressure of 0.1 MPa.

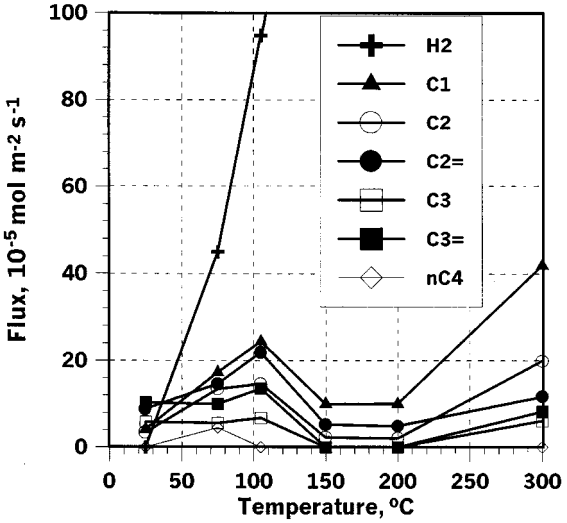

Figure 4. Gas-permeation fluxes under feed-side pressure of 0.168 MPa.

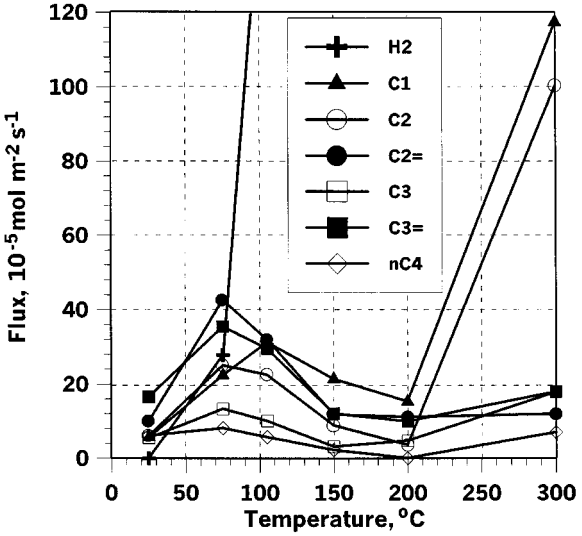

Figure 6. Gas-permeation fluxes under feed-side pressure of 0.372 MPa.

tectable in the permeate stream at the lower feed pressure (0.168 MPa). However, fewer hydrocarbon components were excluded at the higher feed pressure (0.27 MPa). Since the zeolite adsorption is negligible at 500°C for all the components, gas permeation is essentially determined by the diffusivity of the gases in the zeolite pores. Thus, the higher permeation rate of a lighter (or smaller) molecule component is due to its higher diffusivity in the zeolite pores.

To examine the thermal stability of the zeolite membrane and the reproducibility of the permeation data measurement, gas separations were performed on a zeolite membrane at 25–105°C before and after the membrane was heat-treated at 500°C for over two days. Essentially the same separation results were obtained in the two sets of experiments. Furthermore, after heat treatment at 500°C, no appreciable change in the crystal structure was shown in the XRD pattern of the membrane and no crack was found by SEM observation. These indicate good thermal stability of the MFI zeolite membrane and satisfactory reproducibility of data measurements.

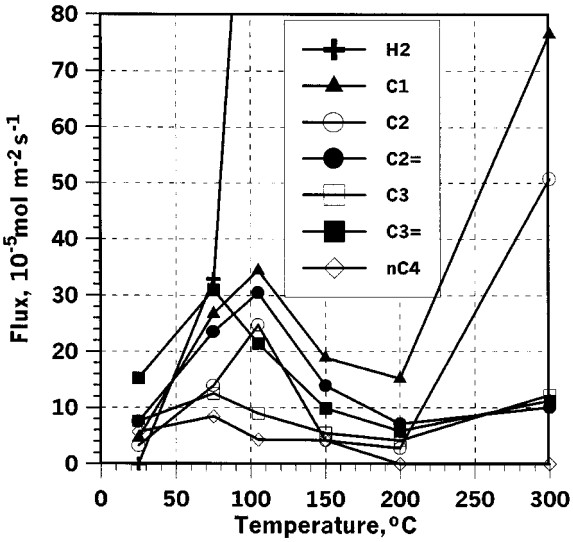

Figure 5. Gas-permeation fluxes under feed-side pressure of 0.27 MPa.

Discussion

We now present a simplified model for the discussion of the separation results just described. It should be noted that numerous efforts have been made to understand the mechanism and develop theoretical models for mass transport through zeolite films (Vroon et al., 1998; Bakker et al., 1997; van de Graaf et al., 1999; Krishna and van de Boeke, 1995; Kapteijn et al., 1995). However, most of the previous work dealt with single-gas permeation. There is no successful model reported in the literature for the quantitative description of multicomponent gas transport through a zeolite membrane. This is in part because of the poor understanding of the adsorbate–adsorbate interaction and configurational interac-

Table 8. Gas Permeation with MFI Membrane at 500°C Under Two Different Feed Pressures*

	0.168 MPa		0.27 MPa	
Component	Flux, 10^{-5} mol/m^2·s	S_i	Flux, 10^{-5} mol/m^2·s	S_i
H_2	1019	3.05	2189	3.24
CH_4	51.53	0.52	107.0	0.41
C_2H_6	10.21	0.29	27.21	0.30
C_2H_4	14.74	0.45	30.00	0.34
C_3H_8	0	0	8.479	0.33
C_3H_6	0	0	17.48	0.35
n-C_4H_{10}	0	0	0	0
i-C_4H_{10}	0	0	0	0

*Other operating conditions: fixed sweep-side pressure of 0.1. MPa; feed flow rates of 11.3 and 10.5 mL/min under feed-side pressures of 0.168 and 0.27 MPa, respectively; and sweep gas flow rates of 13.8 and 17.2 mL/min under feed-side pressures of 0.168 and 0.27 MPa, respectively.

tion between different molecules in the zeolite pores. Furthermore, the microstructure of the polycrystalline zeolite films may change with temperature. Dong et al. (2000) demonstrated that the intercrystal boundaries in the supported polycrystalline zeolite films can be enlarged at high temperature because of the different thermal expansion properties of the zeolite film and the support materials (some zeolite even shrinks with increasing temperature). This further complicates the modeling of multicomponent gas permeation through polycrystalline zeolite membranes.

The simplified model presented next is based on the competitive adsorption and configurational diffusion of permeating species in the zeolite pores. The model is used to correlate the experimental data and will help identify the major characteristic of hydrogen/hydrocarbon separations over the MFI-type zeolite membranes. Furthermore, the model will be used to project performance of the zeolite membrane at higher pressures, at conditions relevant to practical industrial processes but beyond our present experimental capabilities. The simplified model treats the multicomponent system as a binary system with all hydrocarbon compounds in the simulated gas mixture being lumped as one single component, that is, hydrocarbon (HC). The HC passes through the membrane via an adsorption-diffusion mechanism, while hydrogen diffusion is nonadsorptive:

$$J_{\mathrm{HC}} = D_{\mathrm{HC}} \cdot \frac{\Delta C_{\mathrm{HC}}}{l} \tag{4}$$

$$J_{\mathrm{H_2}} = D_{\mathrm{H_2}} \cdot \epsilon \cdot \frac{\Delta P_{\mathrm{H_2}}}{RTl} \tag{5}$$

where J_{HC} and $J_{\mathrm{H_2}}$ are HC and $\mathrm{H_2}$ flux, respectively; D_{HC} and $D_{\mathrm{H_2}}$ are diffusivity of HC and $\mathrm{H_2}$ in the zeolite membrane, respectively; C_{HC} is the amount of adsorbed HC per unit volume of the zeolite membrane; $P_{\mathrm{H_2}}$ is partial pressure of hydrogen; and l is the membrane thickness.

In Eq. 5 ϵ is the fraction of zeolite pores free of hydrocarbons, as

$$\epsilon = 1 - \theta_{HC}, \tag{6}$$

where θ_{HC} is the fraction of zeolite pores filled by hydrocarbons, which is related to HC partial pressure by the Langmuir equation

$$\theta_{\mathrm{HC}} = \frac{C_{\mathrm{HC}}}{C^*_{\mathrm{HC}}} = \frac{K_{\mathrm{HC}} \cdot P_{\mathrm{HC}}}{1 + K_{\mathrm{HC}} \cdot P_{\mathrm{HC}}}, \tag{7}$$

where C^*_{HC} is the maximum amount of HC that can be adsorbed on the zeolite; K_{HC} is the HC adsorption equilibrium constant; and P_{HC} is partial pressure of HC. Equations 4 and 5 assume that the hydrogen diffusion rate in the pores filled with HC is much slower than that in the pores free of HC.

Partial pressures of $\mathrm{H_2}$ and HC in the sweeping side are negligible relative to those in the feed side. This assumption is valid, as the permeation rate is less than 10% of the feed rates in the present experimental setup. Taking the preceding assumption into account, the following flux equations are obtained:

$$J_{\mathrm{HC}} = D_{\mathrm{HC,app}} \cdot \theta_{\mathrm{HC},f} \tag{8}$$

$$J_{\mathrm{H_2}} = D_{\mathrm{H_2,app}} \cdot \left(1 - \theta_{\mathrm{HC},f}\right) \cdot P_{\mathrm{H_2},f} \tag{9}$$

$$\theta_{\mathrm{HC}} = \frac{K_{\mathrm{HC}} \cdot P_{\mathrm{HC},f}}{1 + K_{\mathrm{HC}} \cdot P_{\mathrm{HC},f}}. \tag{10}$$

The temperature dependence of diffusivity and adsorption equilibrium constant are approximated by the following Arrhenius- and van't Hoff-type equations:

$$D_{\mathrm{HC,app}} = A_{\mathrm{HC}} \cdot \exp\left(-\frac{E_{a_{\mathrm{HC}}}}{RT}\right) \tag{11}$$

$$D_{\mathrm{H_2,app}} = A_{\mathrm{H_2}} \cdot \exp\left(-\frac{E_{a_{\mathrm{H_2}}}}{RT}\right) \tag{12}$$

$$K_{\mathrm{HC}} = K_0 \cdot \exp\left(\frac{Q_{\mathrm{HC}}}{RT}\right), \tag{13}$$

where $D_{\mathrm{HC,app}}$ and $D_{\mathrm{H_2,app}}$ are the apparent diffusivity of hydrocarbon and hydrogen, respectively; $\theta_{\mathrm{HC},f}$ is the fraction of zeolite pores adsorbed by HC in the feed side; $P_{\mathrm{HC},f}$ and $P_{\mathrm{H_2},f}$ are partial pressure of HC and $\mathrm{H_2}$ in the feed side, respectively; $E_{a\mathrm{HC}}$ and $E_{a\mathrm{H_2}}$ are the apparent activation energy for HC and $\mathrm{H_2}$ diffusion, respectively; Q_{HC} is the heat of HC adsorption; and K_0 is the preexponential coefficient. From Eqs. 3 and 8–13, the following simple expression of $\mathrm{H_2}$ selectivity can be derived:

$$S_{\mathrm{H_2}} = \frac{D_{\mathrm{H_2,app}}}{K_{\mathrm{HC}} D_{\mathrm{HC,app}}}. \tag{14}$$

In Eq. 14, $S_{\mathrm{H_2}}$ is independent of the total feed pressure and the feed side composition, if $D_{\mathrm{H_2,app}}$, $D_{\mathrm{HC,app}}$, and K_{HC} are temperature dependent only.

Since the model is based on the adsorption–diffusion mechanism, discussions will primarily concern the temperature range of 25–200°C. All permeation data obtained at different temperatures and different feed pressures are regressed by Eqs. 8–13. Resulting parameters are given in Table 9. Heat of adsorption for HC is about 66.3 kJ/mol. This heat of adsorption (for the multicomponent system) is larger than the heat of adsorption data for the individual $\mathrm{C_1}$–$\mathrm{C_4}$ alkanes on pure silicalite crystals calculated from adsorption isotherms of pure species (Sun et al., 1998) (20–55 kJ/mol). This difference is not unexpected considering the differences in the zeolite material and adsorbates in these two studies. Apparent activation energy for HC diffusion is 49.0 kJ/mol, which is consistent with the general understanding that hydrocarbon molecules move inside the zeolite channel through configurational diffusion. Although it has been reported that the hydrogen molecule moves in a manner close to Knudsen diffusion in MFI zeolite pores, activation energy of 9.1 kJ/mol is obtained for hydrogen by regressing the permeation data of this work. This is in agreement with the pure hydrogen permeation behavior reported by Burggraaf et al. (1998).

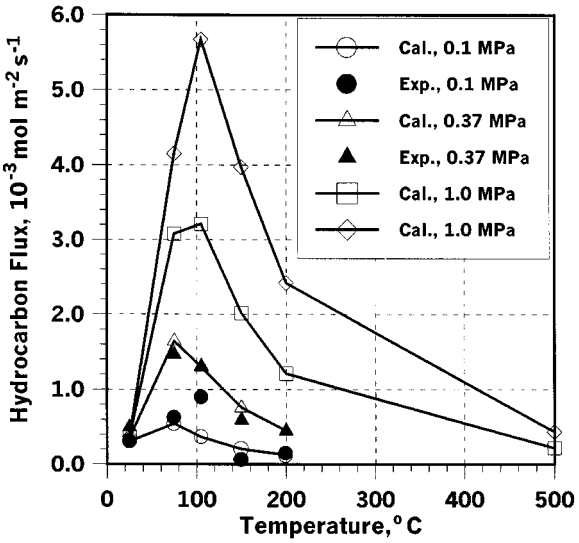

Figure 7. Model projection for variations of hydrocarbon permeation flux with temperature under different feed pressures.

Closed symbols are experimental data.

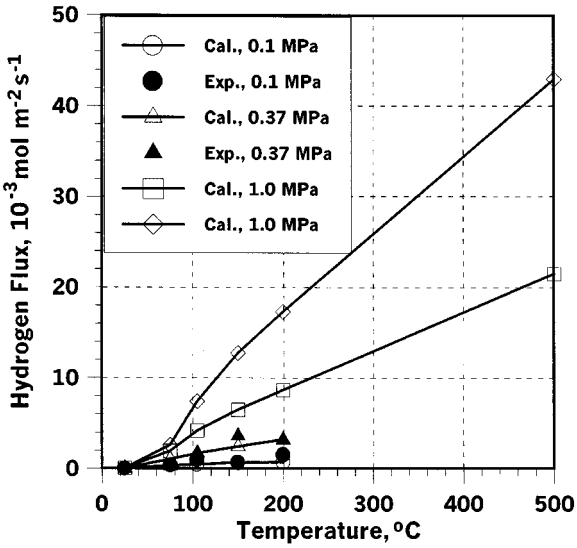

Figure 8. Model projection for variations of hydrogen permeation flux with temperature under different feed pressures.

Closed symbols are experimental data.

Figure 7 shows that under a given feed pressure, HC flux increases, and, after reaching a maximum at about 75°C, decreases with increasing temperature. The model correctly projects this trend. HC adsorption decreases, but the diffusion rate increases with temperature. The bell-shaped flux-temperature profile in the temperature range of 25–200°C is clearly a balanced result of these two opposite driving forces for HC permeation. Most of industrial processes involving H_2/HC mixtures are operated at high pressures (such as above 1.0 MPa). The model projects the same kind of flux-temperature profile when the feed-side pressure is increased. The maximum HC flux increases with the feed-side pressure, and the corresponding temperature tends to shift toward a higher temperature.

Figure 8 shows variation in hydrogen flux with temperature under different feed pressures. Again, the model correctly predicts the trends observed in the experiments. At a given feed pressure, hydrogen flux increases monotonically with temperature. Increasing feed gas pressure shifts the flux-temperature profile toward higher flux direction. At room temperature, hydrogen flux is almost zero (very high selectivity of HC over hydrogen), because the zeolite pores are filled by strongly adsorbed HC. Hydrogen flux increases rapidly, however, and surpasses the HC flux as the temperature is raised. At high temperatures such as 500°C, hydrogen flux is about one to two orders of magnitude higher than the HC flux.

Since the simulated gas mixture (Table 1) contains different concentrations of hydrocarbon molecules, the permeability of individual components is calculated and plotted in Figure 9 against its molecular weight to further illustrate the adsorptive and nonadsorptive separation mechanisms. *iso*-Butane is excluded from the plot, because the shape-selectivity of the silicalite pore plays a key role in *iso*-butane separation. In fact, *iso*-butane permeation was below the GC detection sensitivity in the present work. At low temperatures (25°C), permeability increases with molecular weight. As the temperature rises from 25°C to 105°C, permeability for all components increases, but such a correlation still exists. However, the correlation is completely reversed when the temperature is raised to 500°C. At this temperature, permeability decreases with the molecular weight, because under this condition the diffusivity is the determining factor on permeability.

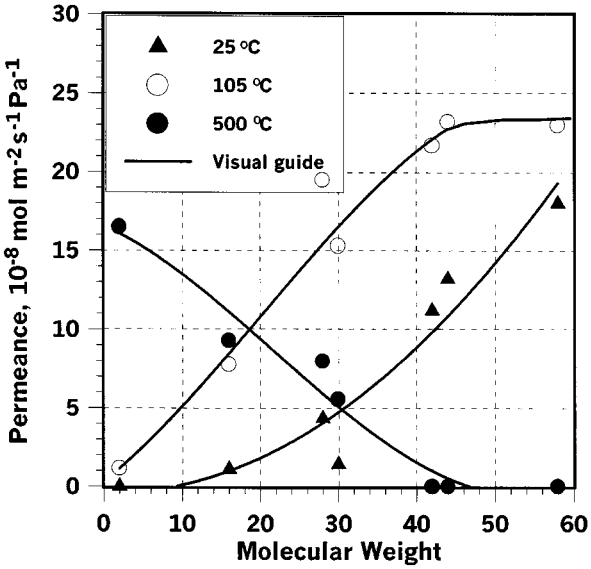

Figure 9. Correlation of permeability of an individual component with its molecular weight at different temperatures.

Feed-side pressure of 0.168-MPa permeate-side pressure of 0.1 MPa with He sweep.

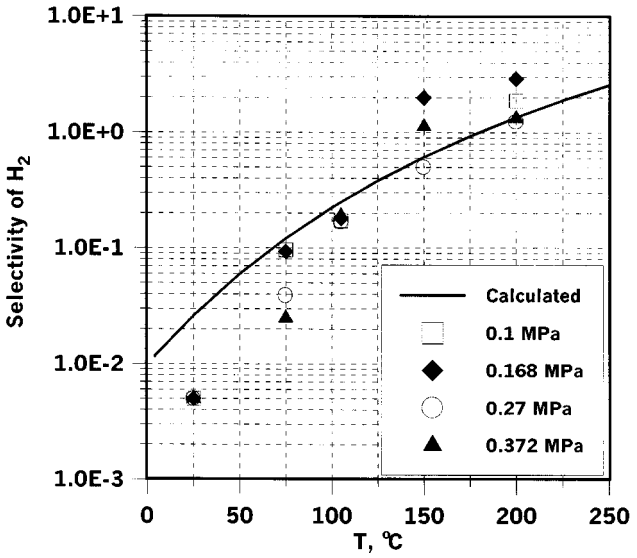

Figure 10. Temperature dependency of the selectivity of hydrogen.

S_{H_2} values at 25°C were estimated according to the GC analysis limits for H_2.

Figure 10 shows the experimental data of hydrogen over hydrocarbon selectivity under different feed pressures and at temperatures below 200°C, where the permeation is dominated by the adsorption–diffusion mechanism. The results predicted by Eq. 14 with the parameters given on Table 9 are plotted in the figure. As shown, the selectivity has a weak dependency on the feed pressure and Eq. 14 correlates the experimental data in the temperature range reasonably well.

Table 10 contains a comparison of the permeation and separation properties of the present zeolite membrane with the well-known microporous carbon membrane developed by Air Products and Chemical Inc. (Rao and Sircar, 1993). The present zeolite membrane shows a much higher hydrocarbon permeance and selectivity than that of the microporous carbon membrane. Furthermore, the carbon membrane loses its selectivity above room temperature because the mechanism of carbon membrane separation is the surface flow, which decreases rapidly with increasing temperature. In contrast, Figures 7 and 8 show that, with the present simulated mixture containing a fairly high concentration of hydrogen (84.5%), the hydrocarbon flux over the zeolite membrane is still higher than hydrogen flux at temperatures up to about 100°C. The present results indicate that the zeolite membrane is an excellent means for efficient separation of hydrogen/hydrocarbon mixtures.

Table 9. Parameters Obtained from Regression for Heat of Adsorption and Activation Energy for Diffusion

	Preexponential Factor	Activation Energy (or Heat of Adsorption) kJ/mol
HC adsorption	6.59×10^{-16} 1/Pa	66.3
HC diffusion	1.43×10^{5} mol/(m^2·s)	49.0
H_2 diffusion	1.06×10^{-7} mol/(m^2·s·Pa)	9.14

Conclusions

Polycrystalline MFI-type zeolite membranes are very effective for separation of multicomponent hydrogen/hydrocarbon mixtures in wide temperature and feed pressure ranges. The hydrocarbon flux exhibits a maximum and minimum profile with respect to temperature variation. In contrast, H_2 flux increases monotonically with temperature. The MFI-type zeolite membrane shows an excellent selectivity for selective rejection of hydrogen from the hydrogen/hydrocarbon mixture at low temperatures (< 100°C). These results suggest that this zeolite membrane can be effectively used for hydrogen concentration/purification of various industrial hydrogen/light-hydrocarbon mixtures. At high temperatures (500°C) the MFI zeolite membrane becomes permselective for hydrogen over hydrocarbons. These properties show a potential for using the zeolite membrane in membrane reactors for hydrocarbon dehydrogenation reactions at high temperatures. The separation results can be characterized by a simple model that assumes an adsorption-control mechanism for hydrocarbon permeation and the configurational gaseous diffusion mechanism for hydrogen permeation over a temperature range of 25–200°C.

Acknowledgment

We are grateful to Amoco Petroleum Co. for supporting the work reported in this article.

Literature Cited

Bai, C., M. Jia, J. L. Falconer, and R. D. Noble, "Preparation and Separation Properties of Silicalite Composite Membranes," *J. Memb. Sci.*, **105**, 79 (1995).

Table 10. Permeation and Separation Properties of Zeolite Membrane Prepared in This Work vs. Carbon Membranes by Rao and Sircar (1993) under Similar Conditions

Gas Component	H_2	CH_4	C_2H_6	C_2H_4	C_3H_8	C_3H_6	n-C_4H_{10}	i-C_4H_{10}
Zeolite membrane*								
Mol fraction (%)	84.5	7.6	2.5	2.5	0.75	1.45	0.4	0.3
Permeance**	0	4.6	15.0	24.5	45.0	70.4	94.7	0
Carbon membrane†								
Mol fraction (%)	41.0	20.2	9.5	0	9.4	0	19.9	0
Permeability††	1.2	1.3	7.7	N/A	25.4	N/A	112.3	N/A
Permeance	0.16	0.17	0.86	N/A	3.3	N/A	14.8	N/A

*Zeolite membrane: $P_f = 0.372$ MPa atm, $P_p = 0.1$ MPa, $T = 25$°C, membrane thickness = 3 μm.
**Unit for permeance (10^{-9} mol/m^2·s·Pa).
†Carbon membrane: $P_f = 0.446$ MPa, $P_p = 0.108$ MPa, $T = 22$°C, membrane thickness = 2.5 μm.
††Reported permeability with unit in (Barrer).

Bakker, W. J. W., F. Kapteijn, J. Poppe, and J. A. Moulijn, ''Permeation Characteristics of a Metal-Supported Silicalite-1 Zeolite Membrane,'' *J. Memb. Sci.*, **117**, 57 (1996).
Bakker, W. J. W., L. J. P. van de Broeke, F. Kapteijn, and J. A. Moulijn, ''Temperature Dependence of One-Component Permeation Through a Silicalite-1 Membrane,'' *AIChE J.*, **43**, 2203 (1997).
Barrer, R. M., ''Porous Crystal Membranes,'' *J. Chem. Soc. Faraday Trans.*, **86**, 1123 (1990).
Burggraaf, A. J., Z. A. E. P. Vroon, K. Keizer, and H. Verweij, ''Permeation of Single Gases in Thin Zeolite MFI Membranes,'' *J. Memb. Sci.*, **144**, 77 (1998).
Coronas, J., J. L. Falconer, and R. D. Noble, ''Characterization and Permeation Properties of ZSM-5 Tubular Membranes,'' *AIChE J.*, **43**, 1797 (1997).
Coronas, J., R. D. Noble, and J. L. Falconer, ''Separation of C_4 and C_6 Isomers in ZSM-5 Tubular Membranes,'' *Ind. Eng. Chem. Res.*, **37**, 166 (1998).
Dong, J., K. Wegner, and Y. S. Lin, ''Synthesis of Submicron Polycrystalline MFI Zeolite Films on Porous Ceramic Supports,'' *J. Memb. Sci.*, **148**, 233 (1998).
Dong, J., and Y. S. Lin, ''In Situ Synthesis of P-type Zeolite Membranes on Porous α-Alumina Supports,'' *Ind. Eng. Chem. Res.*, **37**, 2404 (1998).
Dong, J., Y. S. Lin, M. Z.-C. Hu, R. A. Peascoe, and E. A. Payzant, ''Template Removal Associated Microstructural Development of Ceramic Supported MFI Zeolite Membranes,'' *Mesoporous Microporous Mater.*, **34**, 241 (2000).
Funke, H. H., M. G. Kovalchick, J. L. Falconer, and R. D. Noble, ''Separation of Hydrocarbon Isomer Vapors with Silicalite Zeolite Membranes,'' *Ind. Eng. Chem. Res.*, **35**, 1575 (1996).
Gues, E. R., M. J. den Exter, and H. van Bekkum, ''Synthesis and Characterization of Zeolite (MFI) Membranes on Porous Ceramic Supports,'' *J. Chem. Soc. Faraday Trans.*, **88**, 3101 (1992).
Jia, M., K. V. Peinemann, and R. D. Behling, ''Ceramic Zeolite Composite Membranes. Preparation, Characterization and Gas Permeation,'' *J. Memb. Sci.*, **82**, 15 (1993).
Kapteijn, F., W. J. W. Bakker, G. Zheng, J. Poppe, and J. A. Moulijn, ''Permeation and Separation of Light Hydrocarbons Through a Silicalite-1 Membrane. Application of the Generalized Maxwell-Stefan Equations,'' *Chem. Eng. J.*, **57**, 14 (1995).
Krishna, R., and L. J. P. van de Broeke, ''The Maxwell-Stefan Description of Mass Transport Across Zeolite Membranes,'' *Chem. Eng. J.*, **57**, 155 (1995).
Kikuchi, E., K. Yamashita, S. Hiromoto, K. Ueyama, and M. Matsukata, ''Synthesis of a Zeolite Thin Layer by a Vapor-Phase Transport Method: Appearance of a Preferential Orientation of MFI Zeolite,'' *Microporous Mater.*, **11**, 107 (1997).
Lovallo, M. C., and M. Tsapatsis, ''Preferentially Oriented Submicron Silicalite Membranes,'' *AIChE J.*, **42**, 3020 (1996).
Lovallo, M. C., A. Gouzinizs, and M. Tsapatsis, ''Synthesis of Characterization of Oriented MFI Membranes Prepared by Secondary Growth,'' *AIChE J.*, **44**, 1903 (1998).
Rao, M. B., and S. Sircar, ''Nanoporous Carbon Membranes for Separation of Gas Mixtures by Selective Surface Flow,'' *J. Memb. Sci.*, **85**, 253 (1993).
Sun, M. S., D. B. Shah, H. H. Xu, and O. Talu, ''Adsorption Equilibrium of C_1 and C_4 Alkanes, CO_2 amd SF_6 on Silicalite,'' *J. Phys. Chem. B*, **102**, 1466 (1998).
Vroon, Z. A. E. P., K. Keizer, A. J. Burggraaf, and H. Verweij, ''Preparation and Characterization of Thin Zeolite MFI Membranes on Porous Supports,'' *J. Memb. Sci.*, **144**, 65 (1998).
Vroon, Z. A. E. P., ''Synthesis and Transport Studies of Thin Ceramic Supported Zeolite (MFI) Membranes,'' PhD Thesis, Twente, Univ. of Technology, Enschede, The Netherlands (1995).
Van de graaf, J. M., F. Kapteijn, and J. A. Moulijn, ''Methodological and Operational Aspects of Permeation Measurements on Silicalite-1 Membranes,'' *J. Memb. Sci.*, **144**, 87 (1998).
Van de graaf, J. M., F. Kapteijn, and J. A. Monlijn, ''Modeling Permeation of Binary Mixtures Through Zeolite Membranes,'' *AIChE J.*, **45**, 497 (1999).
Xomeritakis, G., and Y. S. Lin, ''Fabrication of Thin Metallic Membranes by MOCVD and Sputtering,'' *J. Memb. Sci.*, **133**, 217 (1998).
Yan, Y., M. E. Davis, and G. R. Gavalas, ''Use of Diffusion Barriers in the Preparation of Supported Zeolite ZSM-5 Membranes,'' *J. Memb. Sci.*, **126**, 53 (1997).

Manuscript received Jan. 11, 2000, and revision received May 1, 2000.